Inverse modeling of hydraulic tests in fractured crystalline rock based on a transition probability geostatistical approach

Daniela Blessent,[1,2] René Therrien,[1] and Jean-Michel Lemieux[1]

Received 10 June 2011; revised 24 September 2011; accepted 2 November 2011; published 22 December 2011.

[1] This paper presents numerical simulations of a series of hydraulic interference tests conducted in crystalline bedrock at Olkiluoto (Finland), a potential site for the disposal of the Finnish high-level nuclear waste. The tests are in a block of crystalline bedrock of about 0.03 km^3 that contains low-transmissivity fractures. Fracture density, orientation, and fracture transmissivity are estimated from Posiva Flow Log (PFL) measurements in boreholes drilled in the rock block. On the basis of those data, a geostatistical approach relying on a transitional probability and Markov chain models is used to define a conceptual model based on stochastic fractured rock facies. Four facies are defined, from sparsely fractured bedrock to highly fractured bedrock. Using this conceptual model, three-dimensional groundwater flow is then simulated to reproduce interference pumping tests in either open or packed-off boreholes. Hydraulic conductivities of the fracture facies are estimated through automatic calibration using either hydraulic heads or both hydraulic heads and PFL flow rates as targets for calibration. The latter option produces a narrower confidence interval for the calibrated hydraulic conductivities, therefore reducing the associated uncertainty and demonstrating the usefulness of the measured PFL flow rates. Furthermore, the stochastic facies conceptual model is a suitable alternative to discrete fracture network models to simulate fluid flow in fractured geological media.

Citation: Blessent, D., R. Therrien, and J.-M. Lemieux (2011), Inverse modeling of hydraulic tests in fractured crystalline rock based on a transition probability geostatistical approach, *Water Resour. Res.*, *47*, W12530, doi:10.1029/2011WR011037.

1. Introduction

[2] Low-permeability rock formations are investigated for a wide range of applications, such as exploitation of groundwater, mineral, petroleum and geothermal resources, geotechnical and mine engineering issues, and construction of deep geological repositories of high-level spent nuclear fuel, which is the focus of this paper. A geological repository for spent nuclear fuel is a system of natural and engineered barriers whose function is to isolate the spent fuel from humans and the environment. The host rock is the natural barrier while the engineered barriers include the conditioned spent fuel, its container and any external buffer used to isolate the fuel container [*International Atomic Energy Agency*, 1999]. Crystalline rocks have favorable properties for containing radioactive waste, such as high mechanical strength, low permeability, low porosity, low solubility, and good thermal conductivity. However, hydraulically active fractures in crystalline rock enhance its permeability and increase groundwater flow velocities. To evaluate the suitability of a crystalline rock formation to be a natural barrier, it is essential to identify these fractures, characterize their hydraulic properties and develop a conceptual model for fluid flow and solute transport at various spatial scales.

[3] Developing a conceptual model for fractured igneous or metamorphic rock is challenging because the distribution of fractures in the rock mass is often complex. As a result, the spatial distribution of hydraulic conductivity and groundwater fluxes can be very heterogeneous and exhibit sharp spatial transitions because of the discrete nature of the fractures. As mentioned by *Neuman* [2005], suitable conceptual models are discrete fracture network (DFN) with permeable or impermeable matrix blocks [*Bogdanov et al.*, 2003], nonuniform continuum [*Ando et al.*, 2003], or hybrid models of a nonuniform continuum containing a relatively small number of discrete dominant features [*Lee et al.*, 2001]. For all conceptual models, the description can be deterministic or stochastic. While the heterogeneity of fractured rocks can be captured by DFN models, fracture length and connectivity data are often too scarce to build such models. However, specific techniques exist to estimate connectivity of flowing fractures, such as hydraulic and pneumatic tomography [*Hao et al.*, 2008; *Illman et al.*, 2009] or a combined interpretation of cross-hole radar, tracer, and hydraulic data [*Day-Lewis et al.*, 2006]. Equivalent porous medium (EPM) models can be used as an alternative by developing relationships between discrete fracture properties and equivalent porous media properties. However, an equivalent porous medium model generally fails to capture the sharp variation of hydraulic conductivity observed in fractured rock. Indicator or categorical geostatistics using categorical classifications have been proposed to overcome

[1]Department of Geology and Geological Engineering, Université Laval, Quebec, Quebec, Canada.
[2]Now at Department of Civil, Geological and Mining Engineering, École Polytechnique de Montreal, Montreal, Quebec, Canada.

0043-1397/11/2011WR011037

this drawback [*Goovaerts*, 1996] but building realistic models requires a very large amount of field data.

[4] An alternate and promising approach to represent heterogeneous porous media relies on transition probability and Markov chain geostatistics to create a three-dimensional model of categorical facies [*Carle and Fogg*, 1997]. This approach differs from categorical geostatistics in that the model is based on observed transition probabilities of the facies. The approach has been used to represent unconsolidated geological deposits [*Carle and Fogg*, 1997; *Weissmann et al.*, 1999; *Weissmann and Fogg*, 1999] but there are very few applications for fractured rock. In one such application, *Park et al.* [2004] studied a block of crystalline bedrock in the Canadian Precambrian Shield. They defined a relationship between fracture density and transmissivity and then defined five rock facies on the basis of fractured density. Each facies represented a different level of fracture intensity for which hydraulic conductivity was assigned, such as done in the EPM approach. They used the TPROGS software [*Carle*, 1999] to generate conditioned spatial distributions of facies with sequential indicator simulation and simulated quenching. A stochastic EPM model of facies was generated. They simulated flow and transport in the block and successfully calibrated the flow and transport properties of the various rock facies by reproducing hydraulic heads and concentrations measured during tracer tests.

[5] We apply here the transition probability-based geostatistical approach similar to that used by *Park et al.* [2004] to represent background fractures in the crystalline bedrock at Olkiluoto Island, Finland, which is considered for building a deep geological repository for spent nuclear fuel. Unlike *Park et al.* [2004], who investigated uncertainty on predictions of tracer concentrations, we investigate the uncertainty associated with fractured rock properties and we quantify the impact of using flow rates through single fractures to improve model calibration and reduce uncertainty. The objective is to characterize the background fractures with categorical rock types that capture the variability in hydraulic properties without having to resort to the more complex DFN approach. A stochastic distribution of categories, conditioned to field data, is generated for a rock block. The hydraulic properties of the rock categories are then calibrated by reproducing drawdowns and flow rates measured during a series of hydraulic interference tests on open and packed-off boreholes. Previous studies on inverse modeling of hydraulic interference tests in fractured rocks were presented by several authors [*Day-Lewis et al.*, 2000; *Lavenue and de Marsily*, 2001; *Vesselinov et al.*, 2001; *Day-Lewis et al.*, 2006; *Illman et al.*, 2009]. Single-well and multiple-well pumping tests and tracer experiments were used to provide data for model calibration. Inverse modeling was therefore based on observed drawdowns [*Lavenue and de Marsily*, 2001; *Illman et al.*, 2009], pressure records [*Vesselinov et al.*, 2001], or tracer concentrations [*Day-Lewis et al.*, 2006]. In contrast, a unique characteristic of the interference tests considered here is that we combine the use of drawdowns and flow rates. These flow rates were measured with the Posiva Flow Log (PFL) tool [*Rouhiainen and Pöllänen*, 2003] wherever a hydraulically active fracture intersected a borehole. We therefore explore how to use flow rates to improve calibration and also reduce the uncertainty associated with the hydraulic properties of the rock categories. In particular, we compare calibration based only on hydraulic heads and calibration based on both hydraulic heads and flow rates and we quantify reduction in uncertainty of fractured rock properties by using flow rates as targets for calibration. This objective differs from that of *Frampton and Cvetkovic* [2010], who aimed at the characterization of transmissivity for crystalline rock through simulation by conditioning against PFL borehole flow rates. They did not focus on uncertainty of the fractured rock properties.

2. Site Description

[6] The island of Olkiluoto covers an area of 12 km^2 and is located in the Baltic Sea in southwestern Finland (Figure 1). The stratigraphy on the island consists of a thin organic soil layer that overlies unconsolidated overburden that in turn overlies crystalline bedrock. The overburden is mainly glacial till that contains, in order of abundance, fine sand, sand and silt. Its average thickness is 3 m, with a maximum value of 10 m. The crystalline bedrock is mainly gneiss and belongs to the Precambrian Fennoscandian Shield.

[7] Ongoing geological and hydrogeological investigations at Olkiluoto are related to the permanent disposal of spent nuclear fuel in Finland [*Posiva Oy*, 2001]. A total of 52 deep boreholes, whose length ranges from tens of meters to 1 km, were drilled on the island to characterize the crystalline bedrock. The physical properties of the bedrock and the geometry, extent, and connectivity of fractures were characterized from drilling cores, hydraulic tests, groundwater sampling, geophysical surveys and borehole imaging. Major fracture zones identified in the bedrock are defined as having a transmissivity greater than 1×10^{-8} m^2 s^{-1} and a spatial extent of several hundred meters. These fractures, called hydraulic zones (HZ), are subhorizontal and they are the main features of the site-scale hydrostructural model developed for Olkiluoto, which covers a volume of about 20 km^3.

[8] A main component of field investigations at Olkiluoto has been the development and use of the Posiva Hydraulic Test Unit (HTU) [*Klockars et al.*, 2006] and the Posiva Flow Log (PFL) [*Rouhiainen and Pöllänen*, 2003]. The HTU monitors hydraulic head between double packers, as well as below and above packers and provides estimates of hydraulic conductivity at great depths [*Öhberg*, 2006]. Unlike traditional flowmeters that measure the cumulative flow rate along a borehole, the PFL probe measures flow rates in or out of specific borehole sections and therefore locates water conductive fractures that intersect boreholes. The probe consists of an electronic tube, a flow sensor and a flow guide. The guide is fitted with sets of rubber discs tightly pressed against the borehole wall. The distance between the rubber discs defines the test section length, which is typically 2 m, but can be adjusted to any length. Once a measurement is taken, the flow guide is moved down the borehole axis. If the displacement, or measurement increment, is shorter than the test section, overlapping test sections are measured. The detailed flow logging mode uses overlapping test sections to allow for precise identification of the depth of hydraulically conductive fractures along a borehole. The detailed flow logging is performed in small increments, usually a few centimeters, whereas in the

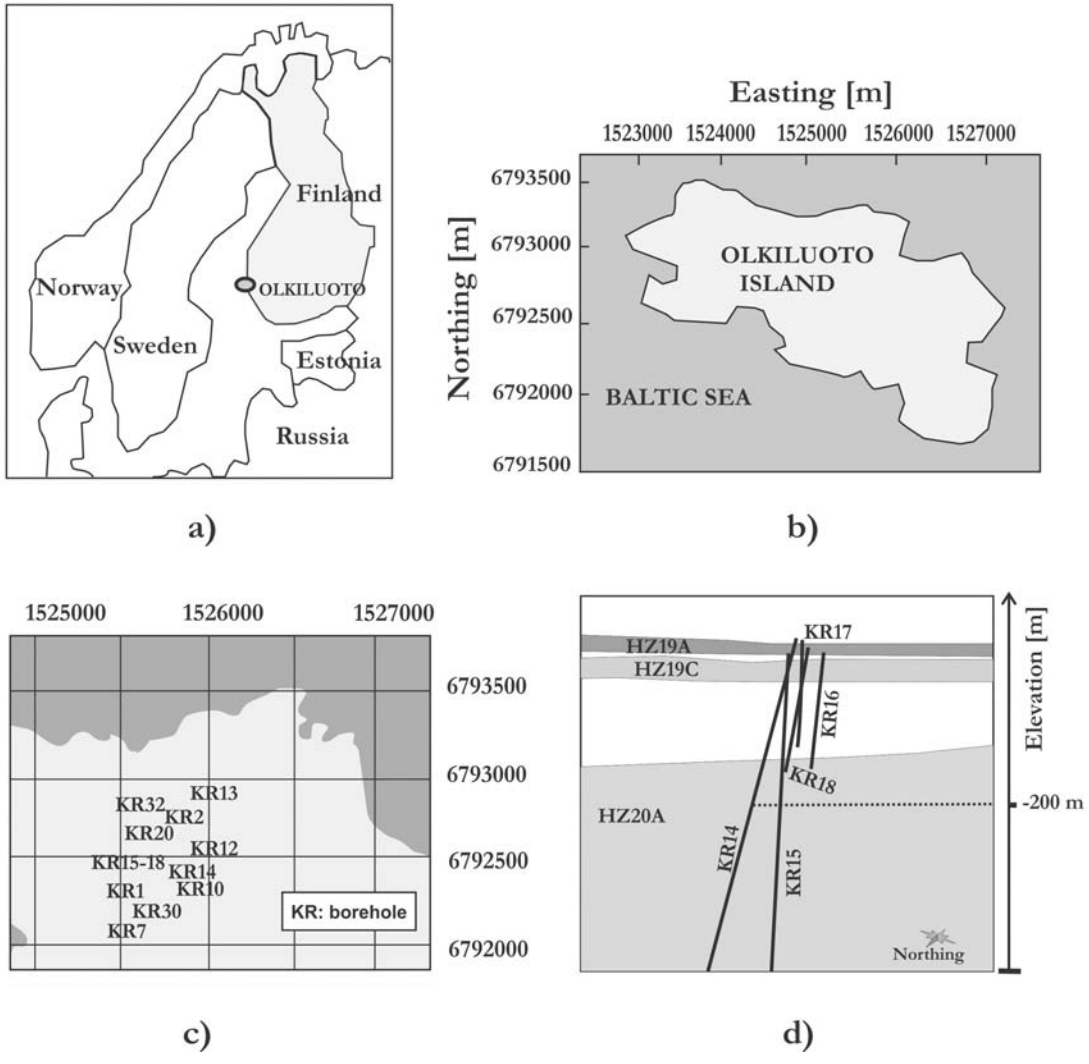

Figure 1. (a) Olkiluoto Island location, (b) Olkiluoto Island shape and extent (UTM coordinates are shown), (c) plan view of the area of interest around boreholes KR14–KR18, and (d) vertical cross section of the KR14–KR18 area with fracture zones HZ19A, HZ19C, and HZ20A and boreholes.

normal logging mode the measurement increment is usually equal to the whole length of the test section without any overlapping with the previous test section [*Öhberg and Rouhiainen*, 2000]. Compared to other borehole logging techniques, the advantages of the PFL are fast measurements and higher resolution, which allows detection of flow rate variations along a borehole that are too small to be measured with conventional flowmeters [*Väisäsvaara et al.*, 2008].

[9] This work focuses on two series of hydraulic interference tests conducted in boreholes KR14, KR15, KR16, KR17, and KR18 that are located in the central area of the island and are referred to as the KR14–KR18 boreholes (Figure 1). These five boreholes are drilled in a cluster and their average horizontal spacing is approximately 45 m. Their depth varies between 130 m to 500 m below ground surface. They are cased from the surface down to a depth of 10 m for KR14 and to a depth of 40 m for KR15–KR18 to prevent flow from the surface to the boreholes. Their lower sections are left open and are therefore in contact with the crystalline bedrock. One shallow borehole is drilled next to each of the KR15–KR18 boreholes. The depth of these four shallow boreholes, KR15B to KR18B, is 45 m and the casing length from ground surface is 10 m. The different casing lengths in deep and shallow B boreholes allow measurements of hydraulic heads in the deeper and shallower portions of the bedrock, respectively.

[10] A first series of tests was conducted between December 2001 and April 2002 in open boreholes. In a first step, single hole tests were conducted in every borehole during which flow rates and drawdown were measured along 2 m sections, with and without pumping the borehole being tested. In the second step, interference tests were conducted where each borehole was pumped in turn and the drawdown and flow rates in the test sections were measured in the other boreholes. The same depth intervals were used both for the single hole tests and the interference tests. The second series of tests was conducted in fall 2004 and, in contrast to the first series described above, boreholes were packed-off and pressure responses were measured in

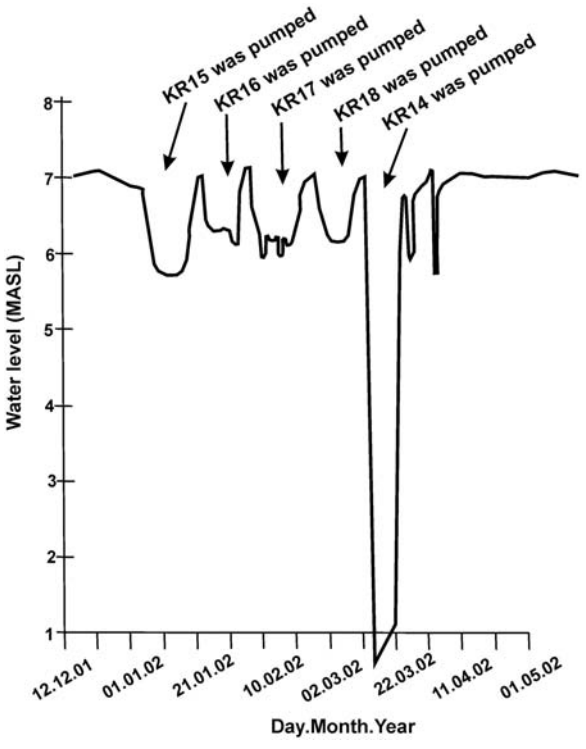

Figure 2. Drawdown at borehole KR14 during the hydraulic interference test (adapted from *Rouhiainen and Pöllänen* [2003]).

the packed-off intervals. Figure 2 shows an example of the drawdown measured at borehole KR14 during the interference tests and indicates that drawdown stabilized quickly, suggesting that quasi steady conditions were achieved during pumping. The hydraulic tests with the HTU were only conducted in boreholes KR14 and KR18 and we therefore only model hydraulic tests where whether KR14 or KR18 are pumped.

3. Fractured Rock Conceptual Model

[11] A stochastic EPM fractured rock facies model is used to define the background fractures located in the block of rock around the KR14–KR18 boreholes. The dimensions of the block are 400, 400, and 200 m in the x, y, and z directions, respectively. The background fractures are defined here as having a spatial extent smaller than one hundred meters and a transmissivity lower than 3×10^{-6} m^2 s^{-1}. These fractures are identified from flow rates measured with the PFL tool during the KR14-KR18 hydraulic tests. The block is bounded at the top by ground surface and the bottom boundary corresponds to the approximate location of subhorizontal fracture zone HZ20A. The rock block also contains subhorizontal fracture zones HZ19A and HZ19C close to ground surface. The spatial extent of these two zones is, however, much larger than that of both the background fractures and the rock block scale considered here and there is also significant uncertainty associated with their location within the rock block. They are therefore not considered to define the conceptual model for the background fractures.

[12] The interpretation of the hydraulic interference tests within the rock block suggests the presence of two hydraulic structures, KR14_4H and Plane-1, whose extents are smaller than that of the Hydraulic Zones, but with transmissivities greater than those of background fractures [*Klockars et al.*, 2006]. Structure KR14_4H has a transmissivity of 3×10^{-5} m^2 s^{-1} and it intersects boreholes KR14, KR15B and KR18B at a depth of about 40 m. Observed water levels show that structure KR14_4H has better flow connection to shallow B boreholes than to the deep KR14–KR18 boreholes [*Vaittinen et al.*, 2003]. Structure Plane-1, in contrast, creates a hydraulic connection between borehole KR14 and the uppermost part of deep boreholes KR15–KR18 and has a transmissivity of 1×10^{-6} m^2 s^{-1} [*Vaittinen et al.*, 2003]. Because the observed hydraulic response during the interference test cannot be adequately represented by highly fractured rock facies only, these large-transmissivity structures are represented as discrete fractures and added to the EPM fractured rock facies conceptual model. The impact of these two discrete fractures on numerical model calibration model is discussed later.

[13] The stochastic conceptual model is developed from background fracture data collected with the PFL tool in boreholes KR14–KR18 and KR15B–KR18B and in 10 other boreholes that are close to the KR14–KR18 cluster. These boreholes are KR1, K2, KR7, KR10, KR12, KR13, KR20, KR20B, KR30, and KR32 (Figure 1). A stereographic projection of the background fracture poles indicates that they are subhorizontal and belong to a single set with a mean orientation of 301°N and a dip of 9° (Figure 3). Because they could not be traced from one borehole to another, the spatial extent of background fractures is assumed to be smaller than the average distance of 45 m between boreholes. Fracture transmissivities were estimated from the measured PFL flow rates using Thiem's or Dupuit's formula, as described by *Väisäsvaara et al.* [2008]. *Frampton and Cvetkovic* [2010], who discussed the use of PFL measurements for inference of field-scale fracture transmissivities, used the same formula with data from the Laxemar site (Sweden). They generated stochastic DFN realizations neglecting porous rock matrix and considering uniform fracture density throughout the model domain. In contrast, we define here EPM fractured rock facies model using the decrease of fracture density with depth observed in the field.

[14] Several relationships have been found or proposed between individual fracture hydraulic properties and other fracture attributes such as length [*Dershowitz et al.*, 2003], depth [*Ingebritsen and Manning*, 1999], strike, and density [*Park et al.*, 2004]. These relationships are, however, not always valid as shown by *Illman* [2005] for unsaturated fractured tuff, where permeabilities and porosities show a lack of correlation with fracture densities. At the Olkiluoto site, there is little information on the length of background fractures such that a relationship between transmissivity and fracture length cannot be established. Fracture transmissivities measured in boreholes tend to decrease with depth but, for the depth reached by the modeled block, the difference in transmissivity with depth is likely insignificant. Moreover, this relationship provides no information on the lateral distribution of the fracture properties.

[15] Another option is to relate EPM hydraulic conductivity to fracture density in the rock mass, which is the approach taken here. There is seldom a definite correlation between fracture density and transmissivity in fractured

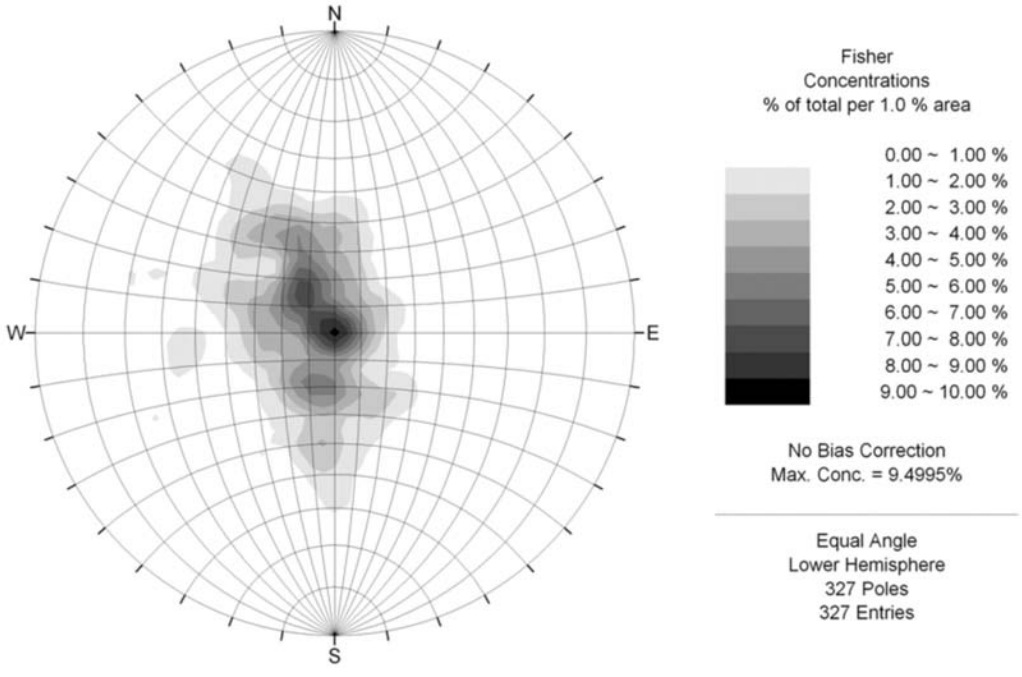

Figure 3. Schmidt equal-area stereographic projection of background fractures poles (strike dip).

rock environments because some fractures are nontransmissive and others are highly transmissive. To overcome this lack of correlation, we have selected only the transmissive fractures to define the fractured rock facies. We therefore consider only the hydraulically active fractures characterized by a flow rate measured with the PFL tool.

[16] The number of transmissive fractures per 5 m interval along the boreholes is identified. The interval length of 5 m chosen here is a tradeoff between a smaller length required to capture the fracture distribution and a larger length required for a mesh resolution appropriate for flow simulations. The transmissivity T_i of a given borehole interval i is the sum of transmissivities T_k of individual fractures k in that interval:

$$T_i = \sum_{k=1}^{n} T_k, \tag{1}$$

where n is the number of fractures in interval i (Figure 4). The resulting plot of transmissivity as a function of fracture density for the 5 m interval length, for all boreholes considered, is shown in Figure 5a. The hydraulic conductivity K is further computed by dividing transmissivity by the interval length Δl (Figure 4) using

$$K_i = \frac{T_i}{\Delta l} \tag{2}$$

and is shown in Figure 5b. The correlation coefficient R^2 between the mean hydraulic conductivity, shown by circles in Figure 5b, and fracture density is 0.91, indicating a statistically significant correlation that supports the categorical geostatistical approach based on fracture density, as used by *Park et al.* [2004].

3.1. Geostatistical Approach

[17] The stochastic equivalent porous medium (EPM) approach used here to represent the fractured rock at the local scale requires the definition of categorical rock facies.

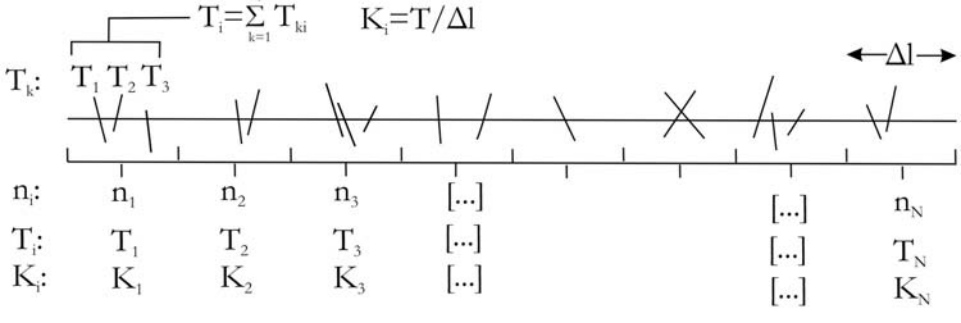

Figure 4. Sketch of the procedure to compute equivalent porous medium (EPM) hydraulic conductivity along borehole intervals, where n_i represents the numbers of fractures for interval i and T and K are transmissivity and hydraulic conductivity, respectively. The length of the interval is Δl.

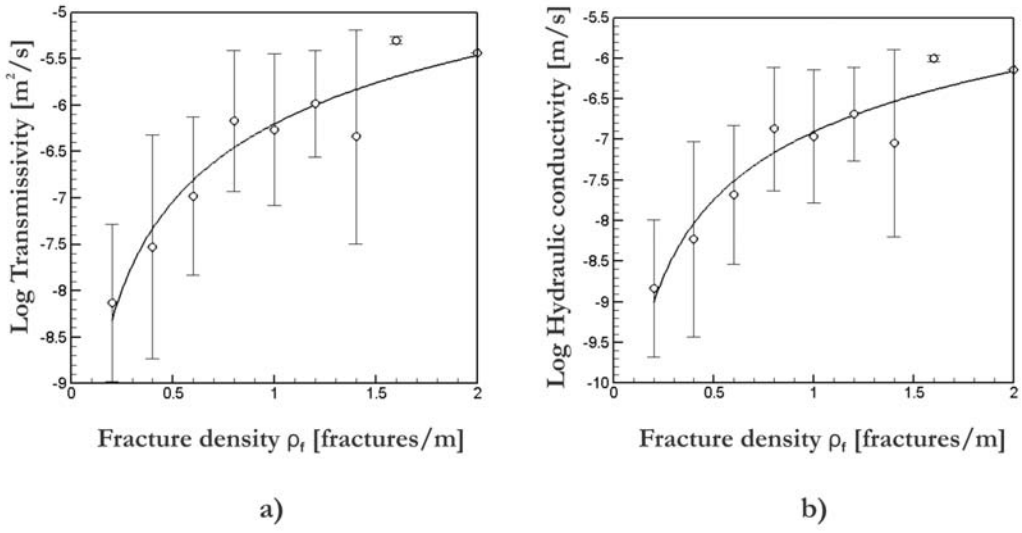

Figure 5. (a) Transmissivity and (b) hydraulic conductivity as a function of fracture density for all borehole intervals considered (interval length is 5 m): circles represent mean values, and bars represent the standard deviation.

The criterion to distinguish a facies from another is its hydraulic conductivity, which is related to the fracture density as shown in Figure 5b. The four facies defined from fracture density are sparsely fractured bedrock (SFB), sparsely to moderately fractured bedrock (SMFB), moderately to highly fractured bedrock (MHFB), and highly fractured bedrock (HFB). The ranges of fracture density and corresponding hydraulic conductivity values for the four facies are given in Table 1.

3.2. Facies Transition Probabilities

[18] Modeling the spatial variability of continuous random functions, such as hydraulic conductivity, is challenging because data are commonly scarce [*Weissmann et al.*, 1999]. For fractured rock, an additional challenge is that hydraulic conductivity does not vary smoothly over space but exhibits sharp variations. Transition probability geostatistics can capture those sharp variations and it was applied to model hydraulic conductivity in crystalline bedrock [*Park et al.*, 2004]. The Transition Probability Geostatistical Software (T-PROGS) [*Carle*, 1999] is used here to generate fractured rock facies distributions in the area surrounding the KR14-KR18 boreholes. Fracture facies defined from fracture density are imported in T-PROGS, which computes transition probabilities of facies as a function of lag distance for a given sampling interval. Markov chains are then fitted to the observed facies transition probabilities. The geostatistical analysis is based on the concept of transition probability t_{jk} between geological facies j and k for two measurement locations separated by distance h_ϕ, which denotes a lag of length h in the direction ϕ. This transition probability is defined as:

$$t_{jk}(h_\phi) = \Pr\{k \text{ occurs at } x + h/j \text{ occurs at } x\} \tag{3}$$

where x is a spatial location vector. Values of $t_{jk}(h_\phi)$ along boreholes reflect the spatial continuity and juxtapositional tendencies of geological facies.

[19] A spatial Markov chain model is used to model the transitional probabilities computed from the observations:

$$\mathbf{T}(h_\phi) = \exp(\mathbf{R}_\phi h_\phi) \tag{4}$$

where $\mathbf{T}(h_\phi)$ denotes a $N \times N$ matrix of transition probabilities and $\mathbf{R}$ is a matrix of transition rates, whose entries represent the rate of change from a category to another one in the direction ϕ.

[20] A detailed description of facies transition probabilities and Markov chains is given by [*Carle*, 1997; *Carle and Fogg*, 1997; *Weissmann et al.*, 1999; *Weissmann and Fogg*, 1999] and is not repeated here.

[21] Equation (3) is used to calculate observed transition probabilities along the boreholes, as shown by dots in Figures 6 and 7. Equation (4) is then used to fit the theoretical Markov chain model to the observed transition probabilities by filling the transition rate matrix **R.** The resulting Markov chain model is shown by the continuous curves. Each

Table 1. Chosen Facies Configuration and Its Properties: Fracture Density Ranges, Mean Facies Transmissivity T, and Mean Hydraulic Conductivity K

Rock Facies Category	Fracture Density Range	Mean log T (m^2 s^{-1})	Mean log K (m s^{-1})
Sparsely fractured bedrock (SFB)	$\rho_f < 0.5$	−7.9	−8.6
Sparsely to moderately fractured bedrock (SMFB)	$0.5 \le \rho_f < 1.0$	−6.5	−7.2
Moderately to highly fractured bedrock (MHFB)	$1.0 \le \rho_f < 1.5$	−5.9	−6.8
Highly fractured bedrock (HFB)	$\rho_f \ge 1.5$	−5.6	−6.3

diagonal element of matrices represents the autotransition probabilities within a category and the asymptote value of the Markov chain model indicates the proportion of the rock facies within the modeled volume. In contrast, off-diagonal elements are the cross-transition probability between categories. The intersection of the tangent to the Markov chain curve with lag axis indicates the mean facies length [*Weissmann et al.*, 1999]. Facies volumetric proportions and mean lengths are listed in Table 2.

[22] There is good fit between observed transitional probabilities and the Markov chain model in the vertical direction, although the model does not capture the exact shape of the observed transition rates (Figure 6). Compared to vertical transitions, the spatial distribution of horizontal transition rates shows greater scatter (Figure 7). The scatter is due to the absence of horizontal continuous facies measurements and the limited number of boreholes. Horizontal facies length could not be observed because there are no horizontal boreholes in the area and because the spacing between the boreholes is larger than the length of the individual fractures. For this reason, other geological evidence is required and a plausible horizontal length is determined from an experimental relationship between fracture transmissivity and length proposed by *Bonnet et al.* [2001] and *Dershowitz et al.* [2003], as well as structural geological mapping across outcrops at Olkiluoto presented by *Paulamäki* [2007]. The estimated mean fracture length is 40 m, which is slightly lower than the average distance of 45 m between boreholes KR14–KR18. This mean length is realistic because background fractures are not assumed to extend across several boreholes. This individual fracture length is translated into a facies length to be used in the Markov chain model, assuming that the facies length is comparable to the length of an individual fracture, at least for facies that are not highly fractured. Thus, the SMFB facies is assumed to have a mean facies length of 40 m, while more intensively fractured facies (MHFB and HFB) are likely to have shorter lengths (20 and 10 m, respectively). The SFB facies is defined as the background facies and its length, computed automatically during the Markov chain fitting process, is approximately 60 m.

3.3. Conditional Simulations

[23] Three-dimensional conditional simulations of fracture facies are created using the Markov chain model along with sequential indicator simulation (SIS) and simulated quenching (SQ) available in T-PROGS. In this study, conditioning data are those located at boreholes KR14–KR18. Alternative configurations are tested using three, four, and five facies defined by different fracture density ranges

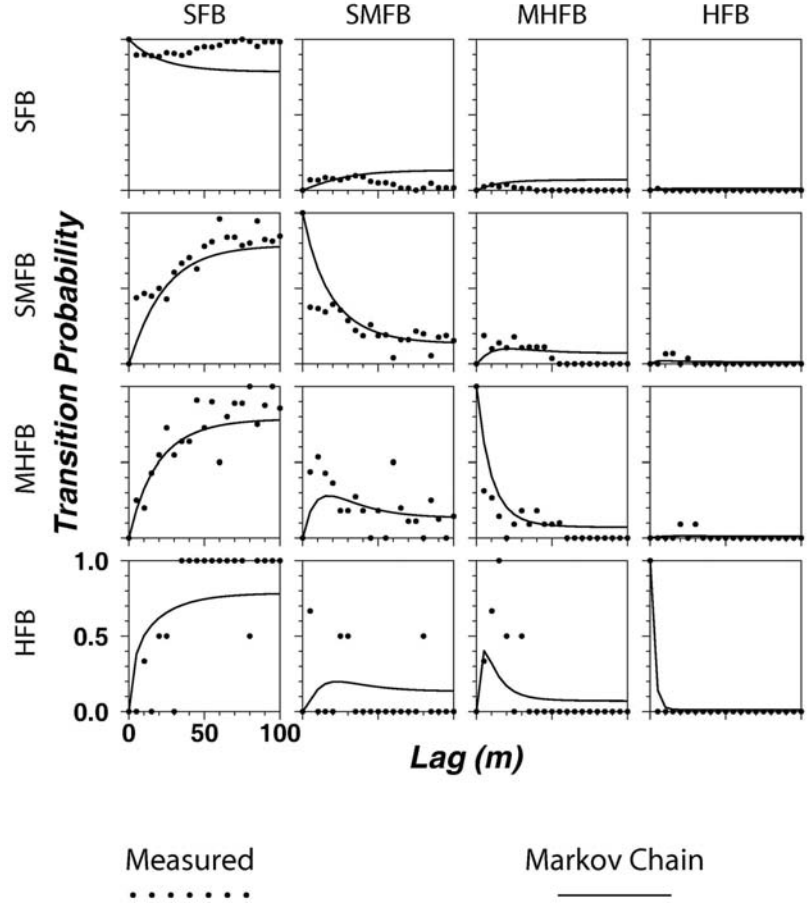

Figure 6. Observed transition probabilities matrix along the vertical direction and fitted Markov chain model.

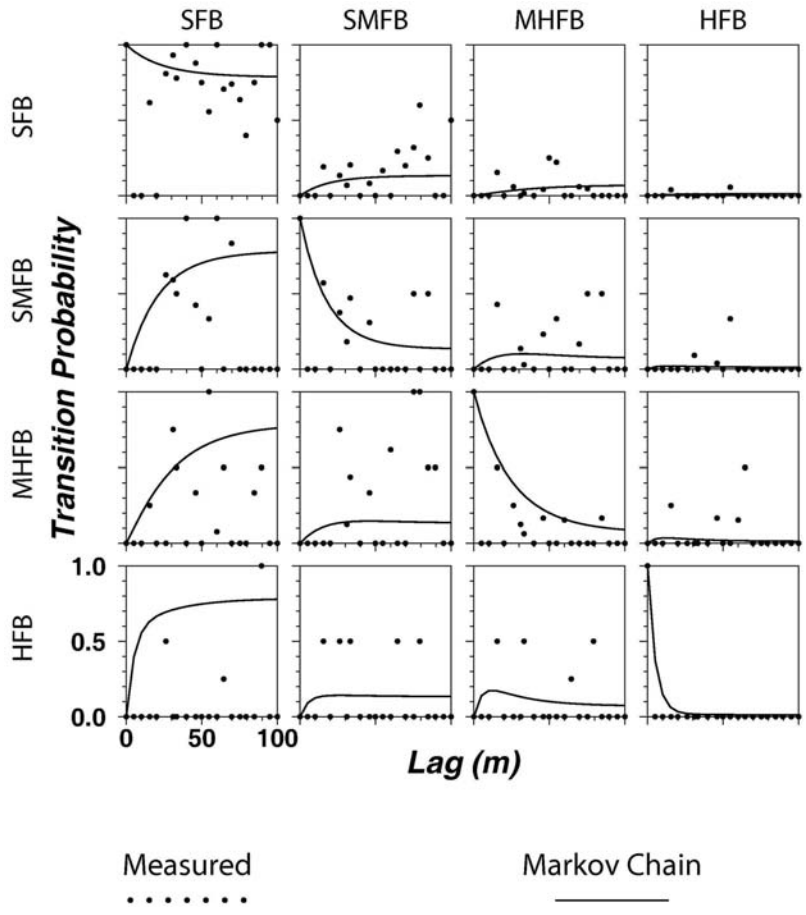

Figure 7. Observed transition probabilities matrix along the horizontal direction and fitted Markov chain model.

(Figure 8). All background fractures shown in Figure 3 are used to obtain the four facies configuration shown in Figure 8c, which is subsequently used for fluid flow simulations. It can be seen that the facies are elongated along a plane that is almost horizontal and characterized by a dip of 9°, which is the average value for the background fractures analyzed. This dip value is low and thus not easily visible because of the coarse cells used, which have edges 5 m long.

[24] As mentioned previously, discrete fractures KR14-4H and Plane-1 are added to the four facies configuration. Two different models are therefore tested for the fluid flow simulations. Model 1 is the stochastic equivalent porous medium model (Figure 9a) and Model 2 is similar to Model 1 except that the two discrete fractures are added (Figure 9b).

Table 2. Statistical Properties of the Fractured Rock Facies

	Facies			
	SFB	SMFB	MHFB	HFB
Proportions (%)	67.93	23.75	6.10	2.22
Mean length (m)				
Vertical	17.2	8.2	7.8	6.8
Horizontal	60.8	40.0	20.0	10.0

4. Numerical Simulation of Fluid Flow

4.1. Numerical Simulator and Model Layout

[25] Fully saturated groundwater flow is simulated with the HydroGeoSphere code [*Therrien et al.*, 2009], which solves coupled surface and subsurface fluid flow and mass transport with the control volume finite element (CVFE) method. Numerical development and governing equations are described in detail by *Therrien et al.* [2009] and are not repeated here.

[26] The computational domain for the flow simulations has dimensions 400 m × 400 m × 200 m in the x, y, and z directions, respectively. The mesh is composed of cubic block elements with a uniform length of 5 m along each of the x, y, and z directions. The mesh generated with HydroGeoSphere has the same spatial extent and resolution than that created with T-PROGS. Boreholes KR14–KR18 and KR15B–KR18B are discretized with one-dimensional line elements. Lines elements coincide with linear edges of the three-dimensional elements and the nodes forming these line elements have the same spatial coordinates as the nodes forming the three-dimensional elements. A one-dimensional fluid flow equation is solved for the line elements and their contributions to flow are added to those from the three-dimensional porous medium elements, as described by *Therrien and Sudicky* [2001]. Open boreholes

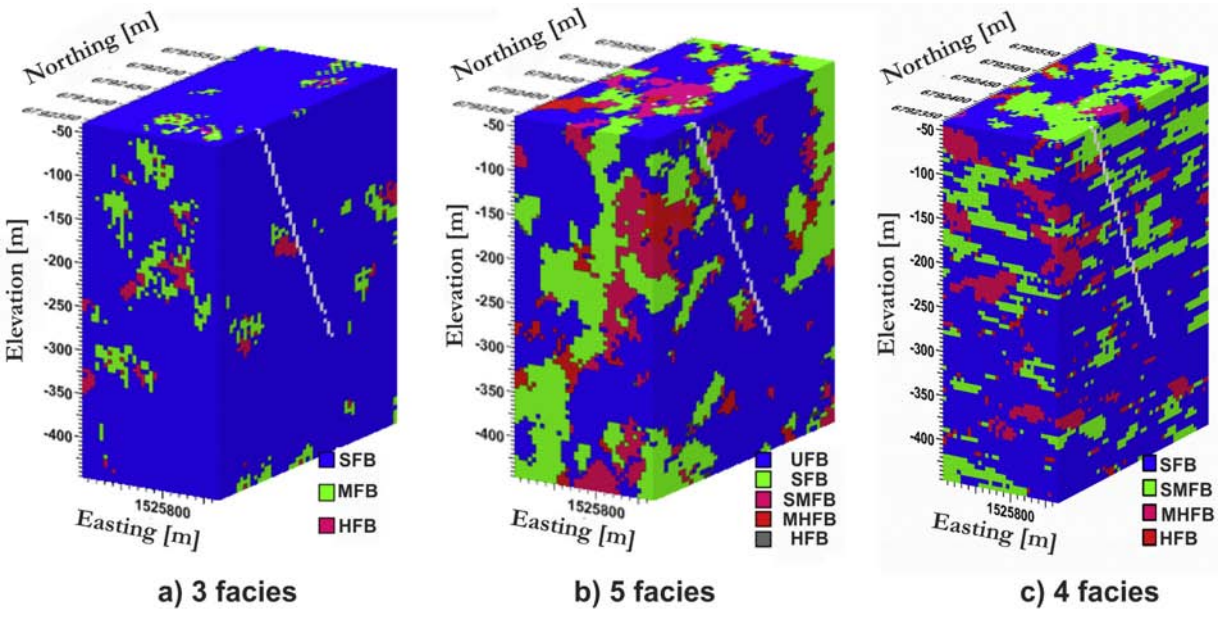

Figure 8. Different geostatistical realizations produced by conditional sequential indicator simulation and simulated quenching based on the three-dimensional Markov chain model (the white cells indicate one of the boreholes where the model is conditioned).

represent high-permeability features embedded into the rock matrix. For model 2, discrete fractures KR14–4H and Plane-1 are represented by two-dimensional quadrilateral elements. Facies hydraulic conductivity and aperture of the two discrete fractures are the calibration parameters. Nevertheless, only the results related to the uncertainty of the facies hydraulic conductivity are presented here, since the focus is on background fractures, which are represented by the fractured rock facies.

[27] Six steady state flow simulation scenarios are considered, as listed in Table 3. Steady state flow is assumed because the crystalline rock has low storage capacity and drawdown stabilized quickly after the start of the test, as shown in Figure 2. The simulations focus on tests where pumping is in KR14 or KR18. Scenario SS_0 represents the natural groundwater flow conditions in the rock block without any borehole. The average values listed in Table 1 are used as hydraulic conductivities of each facies. The other five simulations correspond to hydraulic interference tests and are used to calibrate the facies hydraulic conductivities to reproduce the observed hydraulic heads and PFL flow rates. Scenario SS_1 corresponds to groundwater flow with open boreholes without any pumping. Scenarios SS14_1 and SS18_1 correspond to hydraulic cross hole

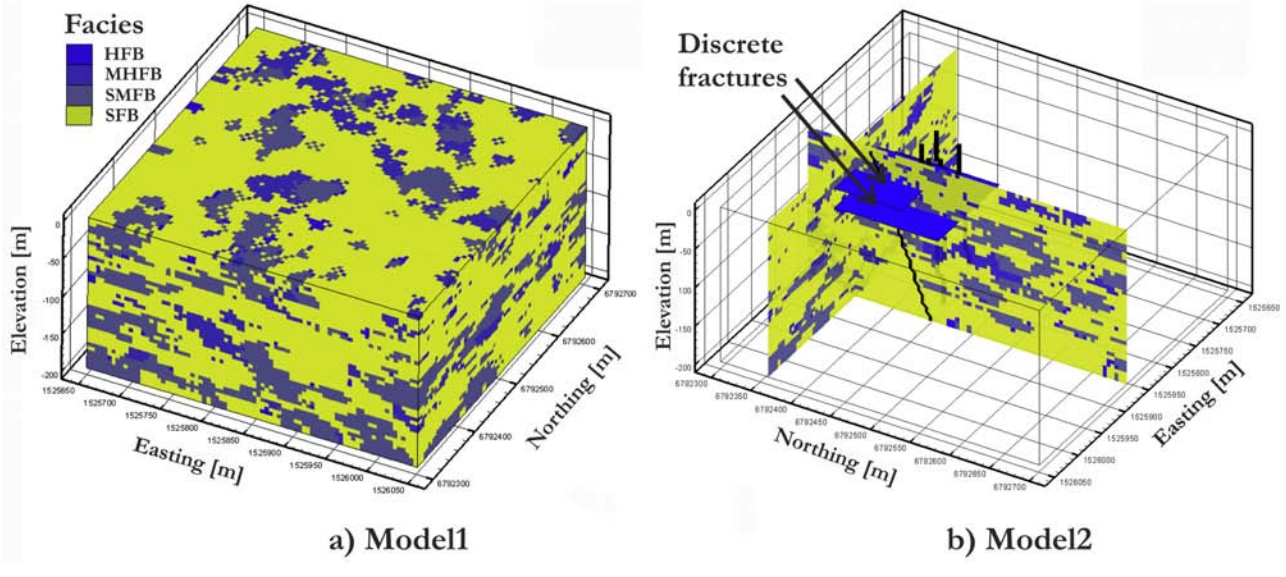

Figure 9. Alternative fractured rock conceptual models tested: (a) only EPM facies and (b) EPM facies and discrete fractures KR14_4H and Plane 1.

Table 3. List of Simulation Scenarios

Name[a]	Description	Boreholes
SS_0	Natural conditions	No boreholes
SS_1	Natural conditions	Boreholes are open and free to cross flow
SS14_1	Pumping in KR14	Boreholes are open and free to cross flow
SS14_2	Pumping in KR14	Boreholes are packed off
SS18_1	Pumping in KR18	Boreholes are open and free to cross flow
SS18_2	Pumping in KR18	Boreholes are packed off

[a]Simulation name SSXX_Y can be read as follows: SS, steady state; XX, pumping borehole; Y, borehole type, where Y = 0 indicates no boreholes, Y = 1 indicates open boreholes, and Y = 2 indicates packed-off boreholes.

interference tests conducted in open boreholes between December 2001 and April 2002 [*Rouhiainen and Pöllänen*, 2003], while scenarios SS14_2 and SS18_2 correspond to hydraulic interference tests performed in packed off boreholes in autumn 2004 [*Klockars et al.*, 2006]. Hydraulic heads computed for scenario SS_1 are used as initial hydraulic heads for the four scenarios where pumping in boreholes KR14 and KR18 is simulated. To compare simulated and observed hydraulic heads, one observation point per open borehole is specified for simulations SS14_1 and SS18_1, while one observation point per section is defined for simulations SS14_2 and SS18_2, where packers separate boreholes in distinct sections. Moreover, to compare simulated and observed flow rates in open boreholes, several observation points are located along borehole axes, depending on the location of the measured PFL flow rates.

[28] Facies SFB represents the background porous rock. It has the largest volumetric proportion such that its hydraulic conductivity is determined by preliminary manual calibration. K_{SFB} is thus not included in the parameter estimation process to reduce computing time for automatic model calibration.

4.2. Inverse Modeling and Parameter Uncertainty Analysis

[29] Parameter Estimation (PEST) software is the nonlinear parameter estimator used for automatic model calibration [*Doherty*, 2004]. Nonlinear relationships are linearized by a Taylor series expansion about the currently best parameter set, which requires the calculation of the derivatives of model-calculated observations with respect to parameters at the beginning of each iteration. Parameter estimation requires that a set of model parameters generates observations that are as close as possible to the set of experimental observations, in the least square sense. This concept is expressed by the objective function Φ, which has to be minimized during the parameter estimation process and which is defined as

$$\Phi = [c - c_0 - J(b - b_0)]^t Q(c - c_0 - J(b - b_0), \quad (5)$$

where $(b - b_0)$ is the parameter upgrade vector, $(c - c_0)$ is the discrepancy, or residual, between the model-calculated observations c_0 and their experimental counterparts c, and Q is a m-dimensional square diagonal matrix whose ith diagonal element is the square of the weight w_i associated to the ith observation. "Trustworthy" observations should have a greater weight than those that cannot be trusted as much and observations of different types, such as hydraulic heads and flow rates, should have different weights such that large numbers do not dominate the parameter estimation process [*Doherty*, 2004].

[30] For inverse groundwater flow simulations, two independent numerical data sets normally exist. The first is a set of observations, such as water levels from wells, and the second is a set of measurements or calculations of the system parameters, such as transmissivity, recharge, discharge, hydraulic conductance. The latter data set is called prior information [*Cooley*, 1983]. The inclusion of prior information is mathematically equivalent to extra measurements and constraints.

[31] Parameter optimization is performed through successive iterations. During each iteration, the numerical model is run several times and the objective function Φ (equation (5)) is evaluated for different values of the parameter upgrade vector (see section 4.2). An iteration ends when Φ is less than 0.3 of its starting value for the current iteration or if its variation is less than 0.01 for two successive evaluations. These numerical values used are among those suggested by *Doherty* [2004].

[32] Optimization termination criteria are based on either the variation of the objective function from one iteration to the next or the behavior of the adjustable parameters. For example, if the reduction of the objective function is less than some prescribed value over a number of successive iterations, calibration execution is stopped. A value of 0.01 for the reduction is chosen here to stop calibration. Calibration is also stopped if successive iterations lead to little change in parameter values. Two iterations and a minimal parameter change per iteration equal to 0.03 are considered here. The maximum number of optimization iterations is set to 25. With the control settings mentioned, more than hundred model calls are required for optimization of model parameters considered here.

[33] Simulations listed in Table 3 are executed successively. The model for scenario SS_1 is calibrated using the hydraulic heads measured in open boreholes. Then, the first pumping scenario SS14_1 is considered. As a first calibration step for that model, only the measured hydraulic heads are considered as targets for calibration. After that, prior information and flow rate measurements are added as targets in the second and third calibration steps, respectively, to analyze their impact on parameter estimation. The model for the second pumping scenario, SS14_2, is calibrated using the hydraulic heads measured in packed-off boreholes. Finally, models for scenarios SS18_1 and SS18_2 are calibrated following the same procedure. Calibration of the model for scenario SS18_1 also include the integration of prior information and flow rate measurements as targets for calibration and it is followed by calibration for scenario SS18_2, with packed-off boreholes.

[34] Linearization in PEST requires calculation of the derivatives of model-calculated observations with respect to calibration parameters. These derivatives must be accurately computed to ensure PEST's success in optimizing parameters. The accuracy in derivatives depends therefore on the accuracy of the computed hydraulic heads and flow

rates, which are here the model-calculated observations. To ensure an accurate flow solution, the absolute convergence criterion for the solution of the discretized flow equation is set to 1.0×10^{-12} m.

4.3. Modeling Results: Natural Groundwater Flow

[35] Steady state natural groundwater flow, without pumping, is simulated without open borehole (Scenario SS_0) and with open boreholes (Scenario SS_1). For the latter, open boreholes KR14-KR18 and KR15B-KR18B are added to the model. The model is only calibrated for scenario SS_1 because there are no observed hydraulic heads for natural flow conditions without boreholes. For scenario SS_1, the calibration targets defined in PEST are the measured hydraulic heads in open boreholes KR14, KR15, KR15B, KR16, KR16B, KR17, KR18, and KR18B.

[36] For these scenarios, the top boundary of the domain represents ground surface and prescribed hydraulic heads corresponding to the interpolated water table elevation are assigned to that boundary. Since water table elevations are not available for the period when the interference tests were conducted, the long-term mean water table elevations are used for the interpolation. Prescribed hydraulic heads are also assigned to the lateral boundaries and the head assigned to all nodes at a given x, y location is that of the top node representing the water table elevation. It is therefore assumed that there is no vertical gradient along the lateral boundaries. As mentioned previously, the bottom boundary coincides approximately with fracture HZ20A, which is assumed to disconnect the shallow and deeper flow regimes representing thus a no-flow boundary.

[37] Simulated hydraulic heads without boreholes, shown in Figure 10a, are clearly influenced by the spatial distribution of rock facies. Compared to the case without open boreholes, computed hydraulic heads for SS_1 are higher around borehole KR14 (Figure 10b) because open boreholes are high-permeability features that create connections between the fractured rock facies and contribute to increase the global hydraulic conductivity of the rock block.

4.4. Modeling Results: Hydraulic Interference Tests

[38] The computed hydraulic heads for scenario SS_1 (Figure 10b) are used as initial hydraulic heads for scenarios SS14_1, SS14_2, SS18_1, and SS18_2 that represent hydraulic interference tests. The lateral and bottom boundary conditions are similar to those used for the scenarios without pumping. A no-flow boundary condition is assigned to the top boundary, which is equivalent to assuming that there is no recharge during the interference tests.

[39] For scenario SS14_1, borehole KR14 is pumped and the other boreholes are open. The pumping rate is 25 L min^{-1} and the measured drawdown at the pumping well is 6 m. The model is first calibrated using the observed hydraulic heads only and the two conceptual models, Model 1 and Model 2, are compared. For Model 1, the residuals are all negative except at borehole KR14 (Figure 11a). In contrast, for Model 2 residuals are more evenly distributed around zero (Figure 11b), which indicates a more reliable calibration than that obtained with Model 1.

[40] To investigate if calibration could be improved by adding prior information (PI) and additional types of targets, additional simulations are attempted with Model 2. Prior information consists in constraining the hydraulic conductivity of the MHFB and HFB facies with respect to that of the SMFB facies according to the following relationships:

$$K_{\mathrm{MHFB}} = 4K_{\mathrm{SMFB}}, \qquad K_{\mathrm{HFB}} = 8K_{\mathrm{SMFB}}, \tag{6}$$

which assume that hydraulic conductivity varies from one facies to another according to the increase in fracture

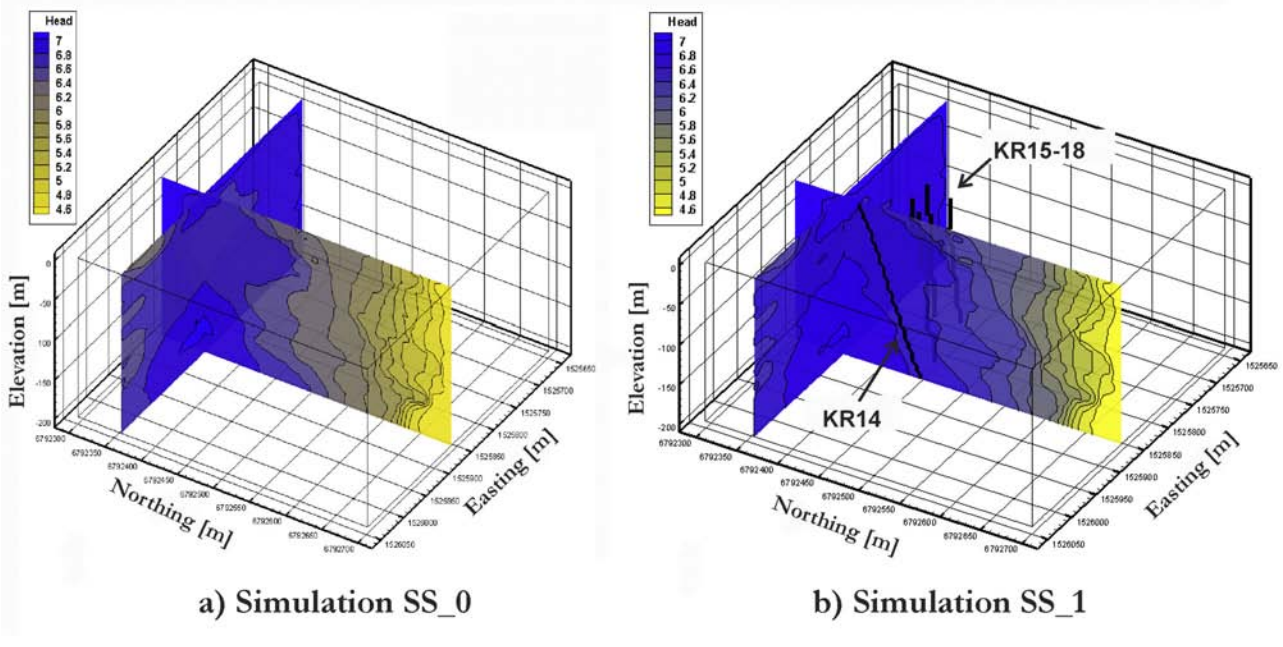

Figure 10. Hydraulic heads for simulations SS_0 and SS_1; slices inside the domain located at x = 1,525,850 m and y = 6,792,350 m are shown.

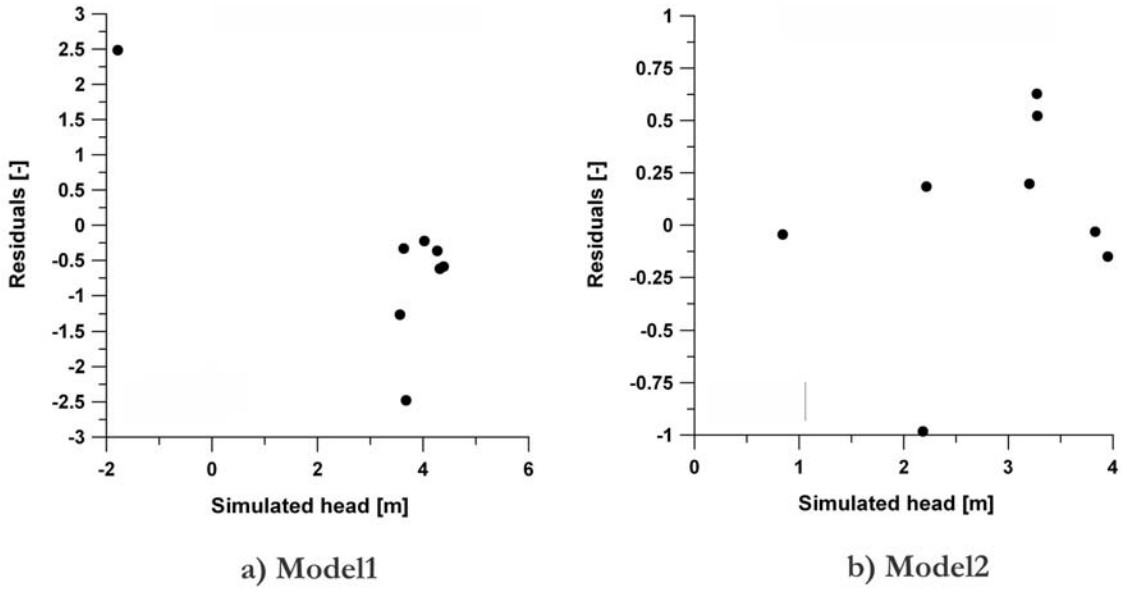

Figure 11. Residuals for simulation SS14_1 with (a) Model 1 (only facies) and (b) Model 2 (facies with two discrete fractures).

density. The ratios between K_{MHFB}/K_{SMFB} and K_{HFB}/K_{SMFB} are obtained from the average hydraulic conductivity values obtained from core observation and PFL measurements (Table 1). These ratios correspond to the trends between K and ρ_f and between T and ρ_f shown in Figure 5.

[41] The additional targets for calibration are the flow rates measured in the boreholes with the PFL tool. Because units for flow rates and hydraulic heads are different, a quantitative distinction between these two types of measurements is required, as indicated by *Doherty* [2004]. This distinction is expressed by different weights assigned to the two types of measurements. In this case, weights equal to 0.1 and 1 are assigned to flow rates and hydraulic heads, respectively, because the magnitude of measured flow rates is usually 1 or 2 orders of magnitude greater than that of hydraulic heads. PFL measurements are available for borehole intervals that are 2 m long, while the spatial resolution of the mesh is 5 m.

[42] Confidence intervals for the calibrated hydraulic conductivities are shown in Figure 12 where the following combinations of calibration targets are compared: only hydraulic heads (Figure 12a), heads and prior information (Figure 12b), only flow rates (Figure 12c), and finally heads, flow rates and prior information (Figure 12d). Regardless of the type of observations considered, the facies with the highest uncertainty is always HFB, which is the facies with the lowest volumetric proportion (Table 2). The largest interval size is for the case when only hydraulic heads are used as targets for calibration. In this case, the upper interval bound for K_{HFB} is 1×10^{-3} m s^{-1} (Figure 12a), which is larger than the hydraulic conductivity of the background fractures at Olkiluoto. Assuming an interval length of 5 m, this hydraulic conductivity corresponds to a transmissivity of 5×10^{-3} m^2 s^{-1}. This value is higher than the highest transmissivities observed at Olkiluoto, which are those of the Hydraulic Zones and are equal to 10^{-4} m^2 s^{-1} [*Vaittinen et al.*, 2003]. Uncertainty is reduced by adding prior information to parameter estimation (Figure 12b) because the relations shown in equation (6) limit the range of variability of calibrated hydraulic conductivities compared to the case without prior information. Confidence intervals are narrower when flow rates are the only targets for calibration (Figure 12c). Therefore, PFL measurements alone may provide more useful information for model calibration than hydraulic heads. When all types of targets are considered, confidence intervals for hydraulic conductivity remain positive (Figure 12d).

[43] For scenario SS14_2, the same withdrawal from borehole KR14 is considered, but the measured drawdown is 6.8 m and observation boreholes are packed off. The results show that the use of prior information alone reduces the interval width and produces a positive value for the lower bound of the hydraulic conductivity interval (Figure 13). Although the confidence intervals are almost similar to those shown in Figure 12d, the parameter correlation coefficients are different. Parameter correlation coefficients are given in a square symmetric matrix of dimension equal to the number of estimated parameters [*Doherty*, 2004]. They are evaluated for each pair of parameters to be estimated and their values may vary from -1 to 1. If prior information is used with hydraulic head measurements in open boreholes only, an extreme correlation between parameters is obtained. When PFL measurements are included as targets for calibration, only one parameter correlation coefficient shows extreme high correlation. When hydraulic heads in packed-off boreholes are used as targets with prior information, three parameter correlation coefficients are greater than 0.95 (Table 4).

[44] In simulation SS18_1, observation boreholes are open and the pumping rate from borehole KR18 is 5.3 L min^{-1}. This withdrawal is much smaller than that considered in borehole KR14 (25 L min^{-1}), but the measured drawdown is 10 m, greater than that measured at borehole KR14. Parameter confidence intervals for this simulation are presented in Figure 14. Uncertainty in parameter estimation

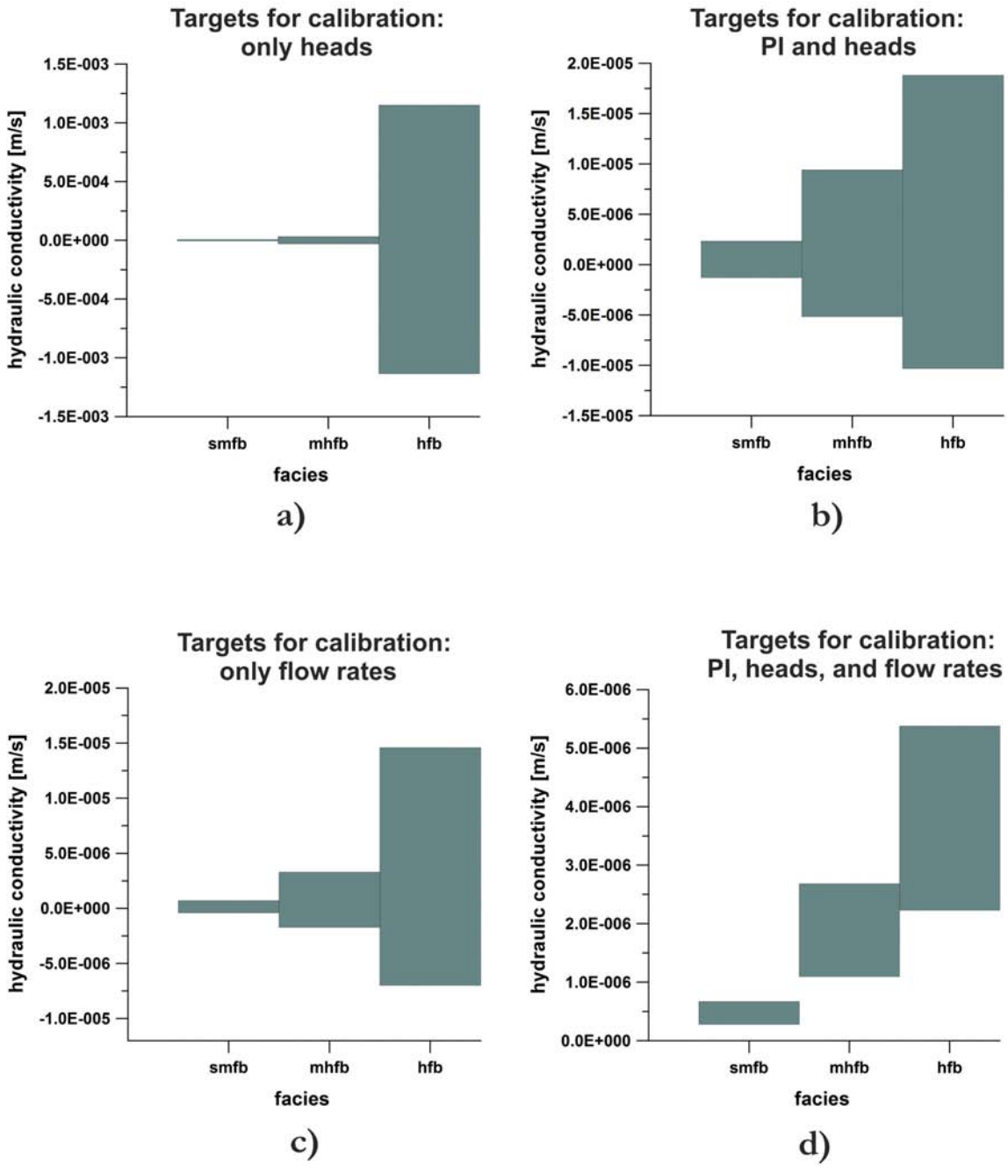

Figure 12. The 95% confidence intervals for the estimated facies hydraulic conductivities for different combinations of measurements used as targets for calibration for simulation SS14_1 (note the y axis is not the same).

is greatly reduced with the combined use of heads, prior information, and flows as targets for calibration, as observed in SS14_1. However, in this case, the lower bounds for the hydraulic conductivity confidence interval are still negative, perhaps as a result of an imprecise characterization of fractured rock around borehole KR18 or high uncertainty associated with measurements. Similar results are obtained for simulation SS18_2 (Figure 15), with packed-off boreholes and a pumping rate equal to 7 L min^{-1}. In this case the measured drawdown is 8.1 m, again greater than that measured during pumping of borehole KR14. The confidence intervals are narrower when prior information is considered but the interval lower bounds are still negative.

[45] Using scenario SS14_1, alternative facies distributions are investigated. T-PROGS is used to generate multiple conditional simulations that have equally probable spatial distributions of random variables or realizations and honor hard data at specified locations. Using the same seed for random generation and the same volumetric facies proportions, ten multiple realizations are computed. Some of

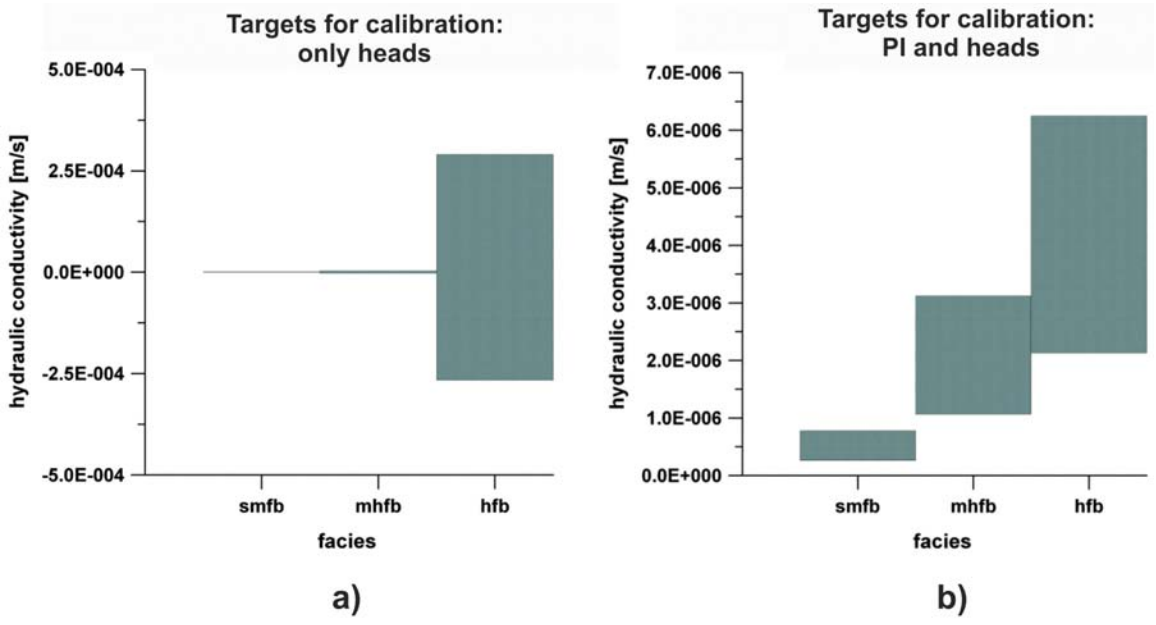

Figure 13. The 95% confidence intervals for the estimated facies hydraulic conductivities obtained from simulation SS14_2 (note the y axis is not the same).

them are illustrated in Figure 16, where sections at x = 1,525,865 m and x = 1,525,840 m show the facies around boreholes KR14 and KR15, respectively. Facies are displayed for each mesh block element, such that contours are square shaped. Thus, regardless of the realization number, the porous rock within 5 m from borehole axis always has the same hydraulic properties, since facies are conditioned at boreholes.

[46] Simulated hydraulic heads at boreholes KR14–KR18 and at some additional observation points are compared for the various realizations. Observation points are located close to each deep borehole, where the facies are conditioned, and in the region between borehole KR14 and KR15, where the drawdown is larger and larger variation in hydraulic head is expected if the facies distribution changes. The computed hydraulic heads are listed in Tables 5 and 6 for the KR14–KR18 boreholes and for the additional observation points, respectively. These results indicate that the largest variance is obtained near pumping well KR14, at observation point named obs1 (Table 6). A large variance is also obtained at boreholes obs6, obs7, and obs8, which are all located near the pumping well, and at the pumping well itself. The variance at other additional observation points (obs2, obs3, obs4, and obs5) is not significant (Tables 5 and 6).

Table 4. Parameter Correlation Coefficients (PCC) Higher Than 0.95 for Pumping in Borehole KR14

Targets for Calibration[a]	Number of PCC $\geq$ 0.95[b]
SS14_1: Only heads	2/10
SS14_1: Heads and PI	6/10
SS14_1: Heads, PFL values, and PI (A and B boreholes)	1/10
SS14_2: Heads and PI	3/10

[a]PFL, Posiva Flow Log; PI, Prior information.
[b]Note that 10 is the total number of parameter correlation coefficients in a [5 × 5] matrix, as in the case considered here, where three facies and two fracture apertures are the estimated parameters.

5. Discussion

[47] The uncertainty in the conceptual model is assessed using either EPM facies with and without discrete fractures. Figure 11 shows that Model 1 does not provide the best match to the observed hydraulic responses during pumping of borehole KR14. The addition of fractures Plane 1 and KR14_4H improves the model calibration. However, the EPM facies model remains a proper representation of background fractures at the rock block scale considered here.

[48] There is uncertainty associated with the boundary conditions used in the model. Assigning prescribed hydraulic heads at the top of the domain, as done for simulations SS_0 and SS_1, does not allow for a proper simulation of drawdown during pumping. Therefore, a no-flow boundary condition is preferred to simulate the hydraulic interference tests. Moreover, in simulations SS_0 and SS_1, the prescribed hydraulic heads vary between 5 and 7 m and simulated values are limited to that range. As a result, for scenario SS_1, simulated hydraulic heads show a very small variation around the average value of 6.8 m, regardless of the facies configuration considered. Finally, for scenarios SS_0 and SS_1, Model 1 and Model 2, described in section 3.3, produce similar hydraulic heads.

[49] For calibration, parameters can be log transformed but it is generally preferable to use nontransformed, or native, values as much as possible to highlight the connection between model results and field data, although the logarithmic transformation produces an inverse problem that converges more easily and prevents the parameter values

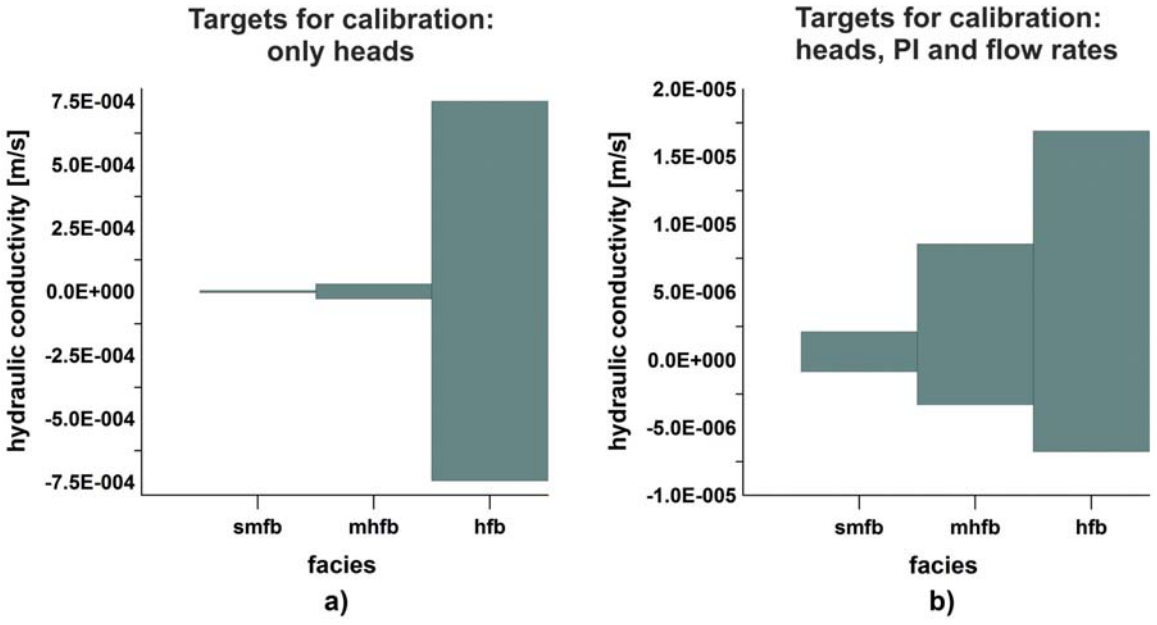

Figure 14. The 95% confidence intervals for the estimated facies hydraulic conductivities obtained from simulation SS18_1 (note the y axis is not the same).

from becoming negative [*Hill and Tiedeman*, 2007]. Since no physical constraints are considered in the parameter estimation process, the estimated parameters may become negative. However, when flow rates are introduced as targets for calibration, the confidence interval length is significantly reduced and negative bounds for the hydraulic conductivity confidence interval are eliminated. This improvement is probably because a match between simulated and measured flow rates out of or into borehole sections requires a positive physical sign for the hydraulic conductivity. Confidence intervals are here deliberately presented for nontransformed parameter values. Logarithmic transformation was attempted, but the interpretation of the resulting intervals was not straightforward. For example, for simulation SS14_1, the lower bounds for the confidence intervals are always positive because of the log transformation, but the whole intervals are much wider compared to the case where the nontransformed parameters are considered, suggesting that native parameters are preferable. One reason may be that PEST computes linear confidence intervals, while the

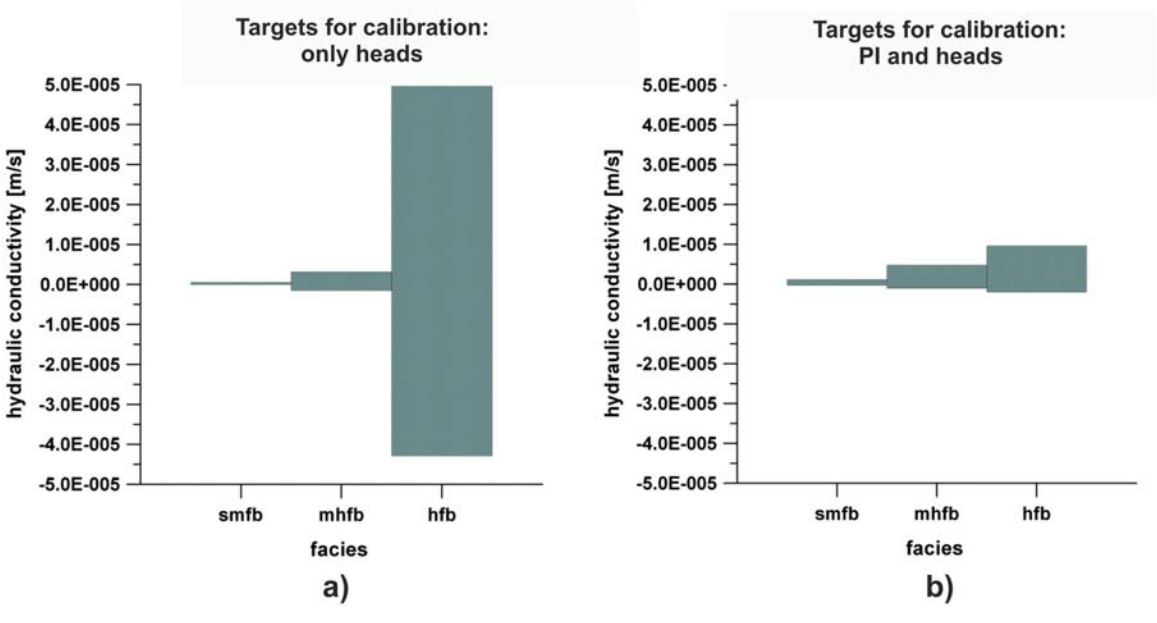

Figure 15. The 95% confidence intervals for the estimated facies hydraulic conductivities obtained from simulation SS18_2 (note the y axis is the same).

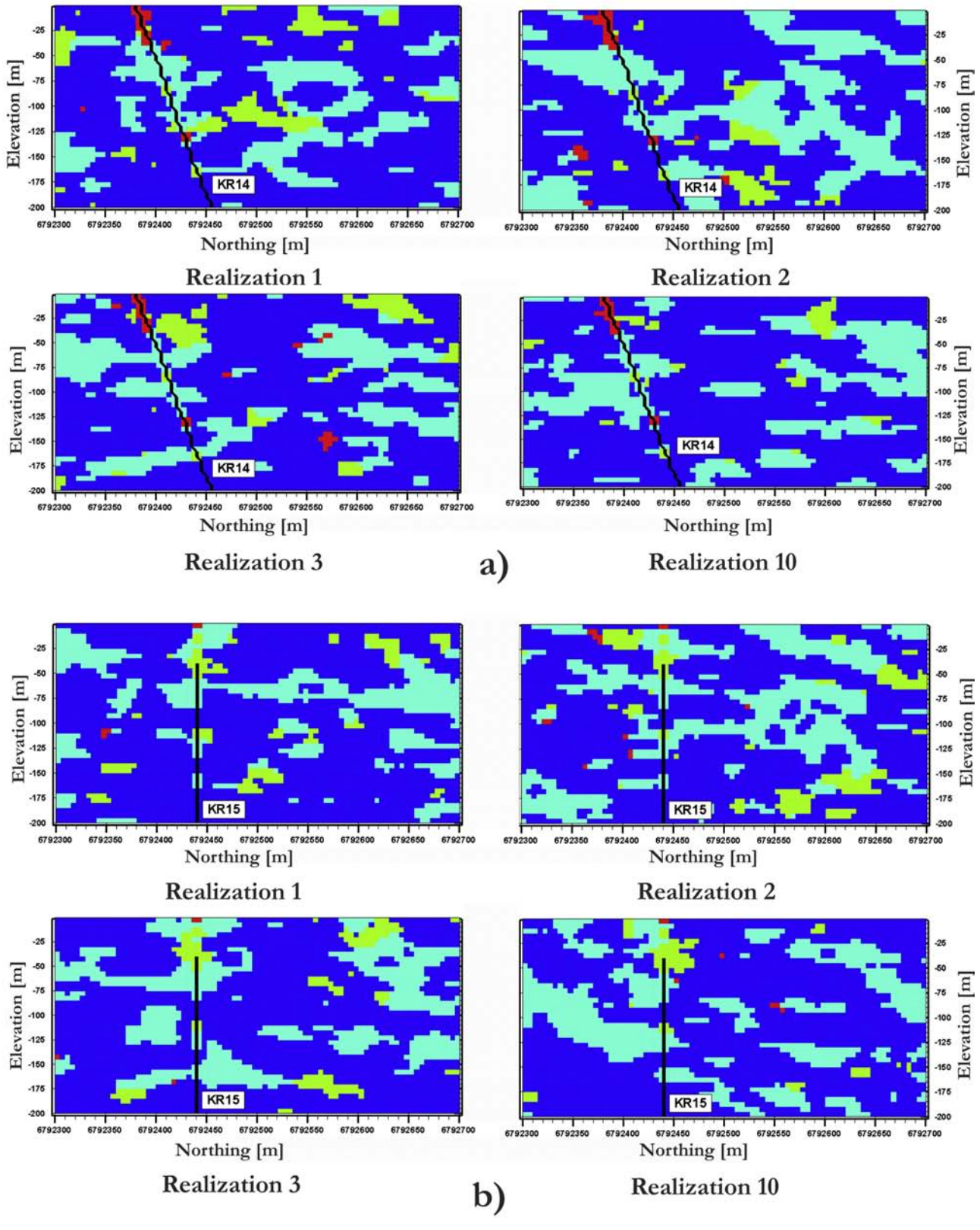

Figure 16. Example of multiple realizations of facies distribution: note the same facies around boreholes (a) KR14 and (b) KR15, which are the conditioned boreholes.

Table 5. Hydraulic Heads (m) Simulated at Boreholes KR14–KR18 for Multiple Realizations of the Same Set of Facies[a]

	Borehole				
	KR14	KR15	KR16	KR17	KR18
x (m)	1,525,865	1,525,840	1,525,795	1,525,810	1,525,825
y (m)	Variable[b]	6,792,440	6,792,425	6,792,455	6,792,435
Realization 1	−5.14	0.22	1.88	1.80	0.96
Realization 2	−1.97	1.40	2.50	2.20	1.60
Realization 3	−4.10	1.30	1.99	2.16	1.60
Realization 4	−6.00	1.20	2.30	2.34	1.75
Realization 5	−2.70	1.40	2.30	2.21	1.70
Realization 6	−3.80	1.20	2.60	2.30	1.50
Realization 7	−2.50	2.06	2.96	2.90	2.40
Realization 8	−2.09	1.80	3.02	2.67	2.19
Realization 9	−5.60	0.62	1.40	1.55	1.05
Realization 10	−2.80	1.60	2.50	2.36	1.90
Variance	2.22	0.29	0.24	0.15	0.20

[a]Variance indicates head variability.
[b]Inclined borehole: y coordinate varies from 6,792,381 to 6,792,549 m.

relationship between hydraulic head and hydraulic conductivity is non linear. Thus, a breakdown in the linearity assumption considered to calculate the confidence intervals may exaggerate the size of the confidence interval.

[50] Confidence intervals are also influenced by the use of prior information, which in turn results in extremely high parameter correlation. For correlation greater than 0.95, parameters may not be estimated uniquely and predictions may be substantially in error [*Anderman and Hill*, 1998]. Therefore, although prior information is useful to calibrate a model, it should be used carefully. Nevertheless, if hydraulic heads and flow rates are considered with prior information, the number of high correlation coefficients may be reduced (Table 4). It is thus recommended to use different types of observation to improve model calibration and parameter estimation.

[51] The PFL measurements are available for borehole sections 2 m long, while the mesh resolution is 5 m. A finer mesh may be used, but in that case the fracture density would be too low, even equal to zero, in most of the borehole intervals. As a consequence, it would be difficult to define facies. With the mesh resolution used, there is therefore some uncertainty associated with the exact location where measurements were made. An additional source of uncertainty is that the sum of PFL measurements taken along a borehole axis is sometimes different from the total withdrawal from the borehole. These uncertainties and the different order of magnitude of the two types of measurements justified a lower weight for flow rates than for hydraulic heads.

[52] For the facies configuration considered here (Table 1), multiple realizations indicate that facies distributions have a larger impact where hydraulic heads show great variation, such as near pumping wells. In contrast, for modest hydraulic head variations, multiple equally probable realizations do not lead to a great difference in head variability between the conditioned boreholes and other locations. The large variance observed at pumping well KR14 (Table 5) is explained by the extension of the drawdown cone. Facies are conditioned around the pumping well, within a radial distance of 5 m from the well axis, but the water removed by pumping comes from a volume that is much larger than the small area around the well axis, where facies are conditioned. If facies, and thus hydraulic properties, vary, some variability in simulation results is expected. The quantification of this variability should be investigated by comparing the results from several conditional simulations that create multiple, equally probable spatial distributions of facies and should be kept in mind when analyzing the uncertainty associated to system along with predictions.

6. Conclusions

[53] We present here the development of a stochastic EPM facies conceptual model for fractured rock and inverse flow modeling of hydraulic interference tests conducted at Olkiluoto Island (Finland). The main objective is to develop an appropriate model for background fractures at local scale and quantify the reduction of uncertainty in the hydraulic properties of the fractured rock by calibrating the model using the measured PFL flow rates. Instead of

Table 6. Hydraulic Heads (m) Simulated at Several Observation Points for Multiple Realizations of the Same Set of Facies[a]

	Close to Deep Boreholes KR14–KR18					Between Boreholes KR14 and KR15		
	obs1 near KR14	obs2 near KR15	obs3 near KR16	obs4 near KR17	obs5 near KR18	obs6	obs7	obs8
x (m)	1,525,870	1,525,835	1,525,800	1,525,815	1,525,820	1,525,860	1,525,840	1,525,840
y (m)	6,792,415	6,792,445	6,792,430	6,792,450	6,792,440	6,792,440	6,792,420	6,792,400
Realization 1	−3.80	0.37	1.85	1.92	1.24	−0.62	−0.86	−0.82
Realization 2	−1.20	1.50	2.45	2.10	1.80	1.40	−1.50	−0.30
Realization 3	−3.40	1.60	1.97	2.00	1.79	1.43	0.13	0.20
Realization 4	−5.30	1.47	2.30	2.10	1.89	0.59	−0.33	−0.51
Realization 5	−1.40	1.49	2.30	2.16	1.90	1.33	0.41	0.46
Realization 6	−1.89	1.29	2.62	2.00	1.57	0.50	0.14	0.17
Realization 7	−1.35	2.10	2.89	2.86	2.60	1.50	0.75	0.38
Realization 8	−0.71	2.00	3.00	2.49	2.26	1.15	1.02	0.55
Realization 9	−3.90	0.99	1.37	1.37	1.23	0.54	−1.10	−1.28
Realization 10	−1.41	1.67	2.50	2.30	2.10	0.91	0.83	0.80
Variance	2.36	0.25	0.24	0.15	0.18	0.43	0.75	0.44

[a]Variance indicates head variability. All observation points are arbitrarily located at a depth of −80 m.

using the more common equivalent porous medium, dual continuum, dual porosity, stochastic continuum or discrete fracture network models, the stochastic EPM facies conceptual model is used here. This model offers an alternate representation of the Olkiluoto bedrock at local scale and avoids building complex and overconnected discrete fracture networks. It is built from background fracture transmissivities and fracture density data, using a geostatistical approach and conditional simulations. Different facies configurations are tested to find the most appropriate one to reproduce the field measurements, such as hydraulic heads and PFL flow rates. Two hydraulic features characterized by higher transmissivity than that of background fractures are represented as discrete fractures and added to the model.

[54] The flow model is calibrated for different scenarios: natural undisturbed flow, pumping in either borehole KR14 or KR18, boreholes either open or packed off. The simulations indicate that PFL flow rates improve model calibration and reduce parameter uncertainty. Moreover, they contribute to provide a unique set of parameter estimates, which is shown by parameter correlation coefficients lower than those obtained for scenarios where PFL flow rates are not considered. Thus, the use of both hydraulic heads and PFL flow rates is recommended to calibrate groundwater flow models for fractured porous rocks, providing that measurements are reasonably precise and accurate. Then, fracture transmissivities estimated from PFL flow rates constitute useful data to build an EPM facies conceptual model, which represents a promising alternative to discrete fracture network models. Finally, multiple equally probable facies realizations show some variability on simulation results, although facies are conditioned at borehole locations. A more detailed analysis will be useful for further understanding of geostatistical methods applied to the representation of heterogeneous geological media.

[55] **Acknowledgments.** We thank the Äspö Task Force Secretariat and Posiva Oy for providing the data and related information on the Olkiluoto site. This work was funded by the Nuclear Waste Management Organization (Canada) and the Natural Sciences and Engineering Research Council of Canada. We thank Bill Lanyon (Fracture Systems Ltd.) for comments and suggestions on a preliminary version of this manuscript, Steven F. Carle for kindly providing the TPROGS code, and Walter Illman and an anonymous reviewer for constructive comments and suggestions.

References

Anderman, E. R., and M. C. Hill (1998), Improving ground-water flow model calibration with the advective-transport observation (ADV) package to MODFLOWP, *U.S. Geol. Surv. Fact Sheet, FS-059-98*.

Ando, K., A. Kostner, and S. P. Neuman (2003), Stochastic continuum modeling of flow and transport in a crystalline rock mass: Fanay-Augères, France, revisited, *Hydrogeol. J.*, *11*(5), 521–535, doi:10.1007/s10040-003-0286-0.

Bogdanov, I. I., V. V. Mourzenko, J.-F. Thovert, and P. M. Adler (2003), Pressure drawdown well tests in fractured porous media, *Water Resour. Res.*, *39*(1), 1021, doi:10.1029/2000WR000080.

Bonnet, E., O. Bour, N. E. Odling, P. Davy, I. Main, P. Cowie, and B. Berkowitz (2001), Scaling of fracture systems in geological media, *Rev. Geophys.*, *39*(3), 347–383.

Carle, S. F. (1997), Integration of geologic interpretation into geostatistical simulation, in *IAMG '97, Proceedings of the Third Annual Conference of the International Society for Mathematical Geology*, edited by V. Pawlowsky Glahn, pp. 711–716, Int. Assoc. for Math. Geol., Barcelona, Spain.

Carle, S. F. (1999), T-PROGS: Transition Probability Geostatistical Software, version 2.1, users guide, 84 pp., Hydrol. Sci. Grad. Group, Univ. of Calif., Davis.

Carle, S. F., and G. E. Fogg (1997), Modelling spatial variability with one and multidimensional continuous-lag Markov chains, *Math. Geol.*, *29*(7), 891–918.

Cooley, R. L. (1983), Incorporation of prior information on parameters into nonlinear regression groundwater flow models: 2. Applications, *Water Resour. Res.*, *19*(3), 662–676.

Day-Lewis, F. D., P. A. Hsieh, and S. M. Gorelick (2000), Identifying fracture-zone geometry using simulated annealing and hydraulic-connection data, *Water Resour. Res.*, *36*(7), 1707–1721, doi:10.1029/2000WR900073.

Day-Lewis, F. D., J. W. Lane, and S. M. Gorelick (2006), Combined interpretation of radar, hydraulic, and tracer data from a fractured-rock aquifer near Mirror Lake, New Hampshire, *Hydrogeol. J.*, *14*(1-2), 1–4, doi:10.1007/s10040-004-0372-y.

Dershowitz, W. S., T. W. Doe, M. Uchida, and J. Hermanson (2003), Correlations between fracture size, transmissivity, and aperture, in *Soil and Rock America 2003*, edited by P. Culligan, H. Einstein, and A. Whittle, *Proc. U.S. Rock Mech. Symp., 39th*, 887–891.

Doherty, J. (2004), PEST: Model-independent parameter estimation user manual, 5th ed., 336 pp., Watermark Numer. Comput., Brisbane, Queensl., Australia.

Frampton, A., and V. Cvetkovic (2010), Inference of field-scale fracture transmissivities in crystalline rock using flow log measurements, *Water Resour. Res.*, *46*, W11502, doi:10.1029/2009WR008367.

Goovaerts, P. (1996), Stochastic simulation of categorical variables using a classification algorithm and simulated annealing, *Math. Geol.*, *28*, 909–921.

Hao, Y., T.-C. J. Yeh, J. Xiang, W. A. Illman, K. Ando, and K.-C. Hsu (2008), Hydraulic tomography for detecting fracture connectivity, *Ground Water*, *46*(2), 183–192, doi:10.1111/j.1745-6584.2007.00388.x.

Hill, M. C., and C. R. Tiedeman (2007), *Effective Groundwater Model Calibration: With Analysis of Data, Sensitivities, Predictions, and Uncertainty*, 455 pp., Wiley-Interscience, Hoboken, N. J.

Illman, W. A. (2005), Type curve analyses of pneumatic single-hole tests in unsaturated fractured tuff: Direct evidence for a porosity scale effect, *Water Resour. Res.*, *41*, W04018, doi:10.1029/2004WR003703.

Illman, W. A., X. Liu, S. Takeuchi, T.-C. J. Yeh, K. Ando, and H. Saegusa (2009), Hydraulic tomography in fractured granite: Mizunami Underground Research site, Japan, *Water Resour. Res.*, *45*, W01406, doi:10.1029/2007WR006715.

Ingebritsen, S. E., and C. E. Manning (1999), Geological implications of a permeability-depth curve for the continental crust, *Geology*, *27*(12), 1107–1110.

International Atomic Energy Agency (1999), Hydrogeological investigation of sites for the geological disposal of radioactive waste, *Tech. Rep. Ser. 391*, Vienna.

Klockars, J., T. Vaittinen, and H. Ahokas (2006), Hydraulic crosshole interference tests at Olkiluoto, Eurajoki in 2004, boreholes KR14-KR18 and KR15B-KR18B, *Work. Rep. 2006-01*, Posiva Oy, Olkiluoto, Finland.

Lavenue, M., and G. de Marsily (2001), Three-dimensional interference test interpretation in a fractured aquifer using the pilot point inverse method, *Water Resour. Res.*, *37*(11), 2659–2675.

Lee, S. H., M. F. Lough, and C. L. Jensen (2001), Hierarchical modeling of flow in naturally fractured formations with multiple length scales, *Water Resour. Res.*, *37*(3), 443–455, doi:10.1029/2000WR900340.

Neuman, S. P. (2005), Trends, prospects and challenges in quantifying flow and transport through fractured rocks, *Hydrogeol. J.*, *13*(1), 124–147, doi:10.1007/s10040-004-0397-2.

Öhberg, A. (2006), Investigation equipment and methods used by Posiva, *Work. Rep. 2006-81*, Posiva Oy, Olkiluoto, Finland.

Öhberg, A., and P. Rouhiainen (2000), Posiva groundwater flow measuring techniques, *Rep. 2000-12*, Posiva Oy, Olkiluoto, Finland.

Park, Y.-J., E. A. Sudicky, R. G. McLaren, and J. F. Sykes (2004), Analysis of hydraulic tracer response tests within moderately fractured rock based on a transition probability approach, *Water Resour. Res.*, *48*, W12404, doi:10.1029/2004WR003188.

Paulamäki, S. (2007), Geological mapping of the region surrounding the Olkiluoto site, *Work. Rep. 2007-30*, Posiva Oy, Olkiluoto, Finland.

Posiva Oy (2001), Nuclear waste management of the Olkiluoto and Loviisa power plants—Annual review, report, Helsinki.

Rouhiainen, P., and J. Pöllänen (2003), Hydraulic crosshole interference test at the Olkiluoto site in Eurajoki, boreholes KR14-KR18 and KR15B-KR18B, *Work. Rep. 2003-30*, Posiva Oy, Olkiluoto, Finland.

Therrien, R., and E. A. Sudicky (2001), Well bore boundary conditions for variably-saturated flow modeling, *Adv. Water Resour.*, *24*, 195–201.

Therrien, R., E. A. Sudicky, R. G. McLaren, and S. M. Panday (2009), HydroGeoSphere: A three-dimensional numerical model describing fully-integrated subsurface and surface flow and solute transport, user's guide, 392 pp., Groundwater Simul. Group. Waterloo, Ontario, Canada.

Väisäsvaara, J., S. Kristiansson, J. Pöllänen, and M. Sokolnicki (2008), Monitoring measurements by the difference flow method during the year 2007, drillholes OL-KR2, KR7, KR8, KR14, KR22, KR22B, KR27 and KR28, *Work. Rep. 2008-40*, Posiva Oy, Olkiluoto, Finland.

Vaittinen, T., et al. (2003), Bedrock model of the Olkiluoto site, version 2003/1, report, Posiva Oy, Olkiluoto, Finland.

Vesselinov, V. V., S. P. Neuman, and W. A. Illman (2001), Three-dimensional numerical inversion of pneumatic cross-hole tests in unsaturated fractured tuff: 1. Methodology and borehole effects, *Water Resour. Res.*, *37*(12), 3001–3018, doi:10.1029/2000WR000133.

Weissmann, G. S., and G. E. Fogg (1999), Multi-scale alluvial fan heterogeneity modeled with transition probability geostatistics in a sequence stratigraphic framework, *J. Hydrol.*, *226*, 48–65.

Weissmann, G. S., S. F. Carle, and G. E. Fogg (1999), Three-dimensional hydrofacies modeling based on soil surveys and transition probability geostatistics, *Water Resour. Res.*, *35*(6), 1761–1770.

D. Blessent, Department of Civil, Geological and Mining Engineering, École Polytechnique de Montreal, C.P. 6079, Succ. Centre-ville, Montreal, QC H3C 3A7, Canada.

J.-M. Lemieux and R. Therrien, Department of Geology and Geological Engineering, Université Laval, Quebec, QC G1V 0A6, Canada. (rene.therrien@ggl.ulaval.ca)